AIP Journal of Applied Physics

Analytical model for reduction of deep levels in SiC by thermal oxidation

Koutarou Kawahara, Jun Suda, and Tsunenobu Kimoto

Citation: J. Appl. Phys. **111**, 053710 (2012); doi: 10.1063/1.3692766
View online: http://dx.doi.org/10.1063/1.3692766
View Table of Contents: http://jap.aip.org/resource/1/JAPIAU/v111/i5
Published by the American Institute of Physics.

Related Articles

Effect of defect bands in β-In2S3 thin films
J. Appl. Phys. 111, 093714 (2012)

Defect energy levels and electronic behavior of Ni-, Co-, and As-doped synthetic pyrite (FeS2)
J. Appl. Phys. 111, 083717 (2012)

Defect level distributions and atomic relaxations induced by charge trapping in amorphous silica
Appl. Phys. Lett. 100, 172908 (2012)

First principles study of the oxygen vacancy formation and the induced defect states in hafnium silicates
J. Appl. Phys. 111, 074106 (2012)

First-principles study of impurities in TlBr
J. Appl. Phys. 111, 073519 (2012)

Additional information on J. Appl. Phys.

Journal Homepage: http://jap.aip.org/
Journal Information: http://jap.aip.org/about/about_the_journal
Top downloads: http://jap.aip.org/features/most_downloaded
Information for Authors: http://jap.aip.org/authors

ADVERTISEMENT

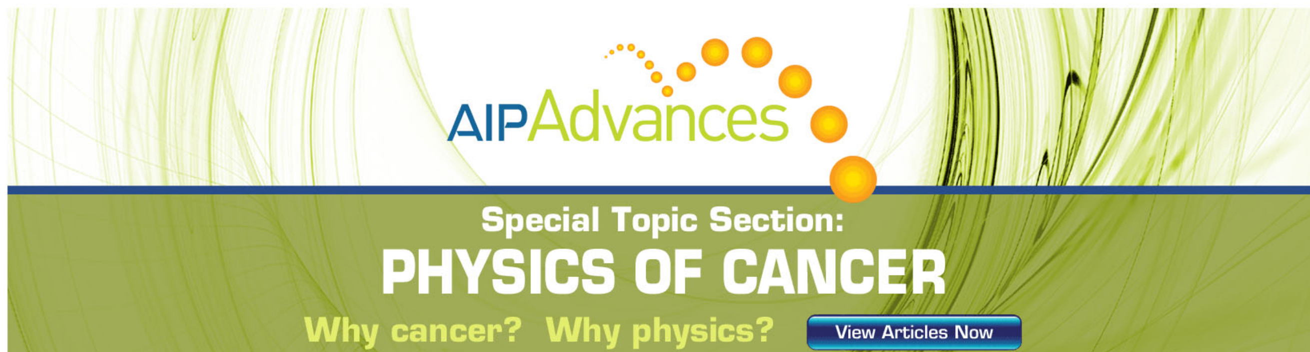

Downloaded 07 May 2012 to 130.54.110.71. Redistribution subject to AIP license or copyright; see http://jap.aip.org/about/rights_and_permissions

JOURNAL OF APPLIED PHYSICS 111, 053710 (2012)

Analytical model for reduction of deep levels in SiC by thermal oxidation

Koutarou Kawahara,[a)] Jun Suda, and Tsunenobu Kimoto[b)]
Department of Electronic Science and Engineering, Kyoto University, Katsura, Nishikyo, Kyoto, 615-8510, Japan

(Received 12 January 2012; accepted 6 February 2012; published online 14 March 2012)

Two trap-reduction processes, thermal oxidation and C^+ implantation followed by Ar annealing, have been discovered, being effective ways for reducing the $Z_{1/2}$ center ($E_C - 0.67$ eV), which is a lifetime killer in n-type 4H-SiC. In this study, it is shown that new deep levels are generated by the trap-reduction processes in parallel with the reduction of the $Z_{1/2}$ center. A comparison of defect behaviors (reduction, generation, and change of the depth profile) for the two trap-reduction processes shows that the reduction of deep levels by thermal oxidation can be explained by an interstitial diffusion model. Prediction of the defect distributions after oxidation was achieved by a numerical calculation based on a diffusion equation, in which interstitials generated at the SiO_2/SiC interface diffuse to the SiC bulk and occupy vacancies related to the origin of the $Z_{1/2}$ center. The prediction based on the proposed analytical model is mostly valid for SiC after oxidation at any temperature, for any oxidation time, and any initial $Z_{1/2}$-concentration. Based on the results, the authors experimentally achieved the elimination of the $Z_{1/2}$ center to a depth of about 90 μm in the sample with a relatively high initial-$Z_{1/2}$-concentration of 10^{13} cm^{-3} by thermal oxidation at 1400 °C for 16.5 h. Furthermore, prediction of carrier lifetimes in SiC from the $Z_{1/2}$ profiles was realized through calculation based on a diffusion equation, which considers excited-carrier diffusion and recombination in the epilayer, in the substrate, and at the surface. © *2012 American Institute of Physics*. [http://dx.doi.org/10.1063/1.3692766]

I. INTRODUCTION

SiC has attracted increasing attention as a promising wide-bandgap semiconductor for realizing high-power, high-temperature, and high-frequency devices. One of the dominant obstacles to realizing high-performance SiC devices is existence of deep levels in SiC epilayers. Deep levels are generated during epitaxial growth[1–4] and device fabrication steps such as ion implantation[5–10] and reactive ion etching.[11] The deep levels work as recombination centers resulting in reduction of the carrier lifetime[12] and also work as carrier traps, leading to reduction of the conductivity. Therefore, deep levels, especially the $Z_{1/2}$ center, a well known deep level that is a lifetime killer in n-type 4H-SiC,[13,14] must be controlled. The typical carrier lifetime for commercially available SiC epilayers is only 0.6-1 μs due to the high $Z_{1/2}$ concentration of about 10^{13} cm^{-3}, while over 5 μs lifetime is required for 10 kV PiN-diodes.

The origin of $Z_{1/2}$ center has been extensively investigated.[1,3,15,16] The authors speculate that $Z_{1/2}$ center is a carbon-vacancy (V_C)-related defect because of the following three experimental results. First, the $Z_{1/2}$ center is generated by low-energy (100–200 keV) electron irradiation, which displaces only C atoms, without subsequent annealing.[3,15] Second, the $Z_{1/2}$ concentration is lower in the samples grown under C-rich condition (higher C/Si ratio).[17] Third, the $Z_{1/2}$ is a thermally stable defect,[1] showing no change of concentration up to 1600 °C,[3] at which temperature interstitials can easily diffuse. Additionally, it has been reported that the energy levels and the negative U nature originating from V_C obtained by *ab initio* calculation (density functional theory) are in agreement with the properties of the $Z_{1/2}$ center detected by deep level transient spectroscopy (DLTS).[18]

There are two effective methods to reduce the $Z_{1/2}$ center: (i) C^+ implantation followed by Ar annealing[19,20] and (ii) thermal oxidation.[21] In the case of the C^+-implantation process, implanted excess carbon atoms should diffuse to the deeper region of an SiC epilayer during post-implantation annealing and fill V_C, resulting in reduction of the $Z_{1/2}$ concentration.[20] In the case of thermal oxidation, the $Z_{1/2}$ reduction may be ascribed to diffusion of interstitials generated at the SiO_2/SiC interface during oxidation[21] as shown in Fig. 1. There are several reports indicating the generation of interstitials at the SiO_2/SiC interface,[22–24] which support this trap reduction model. (i) Experimental oxidation rate of SiC can be well simulated by considering silicon and carbon emission from the oxidation interface.[22] (ii) An increase of carbon atom concentration at the SiO_2/SiC interface was observed by electron energy loss spectroscopy.[23] (iii) It has been predicted from *ab initio* calculation that carbon clusters are formed at the SiO_2/SiC interface during oxidation.[24] The trap reduction mechanism by thermal oxidation, however, has not been fully understood.

The purposes of this study are to ascertain the trap-reduction model shown in Fig. 1 and to enable prediction of the depth profiles of deep levels after oxidation in order to control deep levels by thermal oxidation. For these purposes, the authors compare deep levels in the SiC epilayers after the C^+-implantation process and those after thermal oxidation, and investigate the oxidation-temperature dependence,

[a)]Electronic mail: kawahara@semicon.kuee.kyoto-u.ac.jp.
[b)]Also at Photonics and Electronics Science and Engineering Center (PESEC), Kyoto University.

 © 2012 American Institute of Physics

Downloaded 07 May 2012 to 130.54.110.71. Redistribution subject to AIP license or copyright; see http://jap.aip.org/about/rights_and_permissions

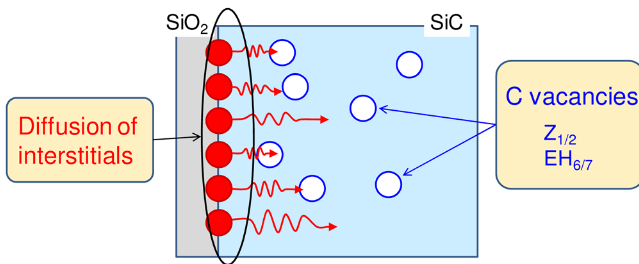

FIG. 1. (Color online) Schematic model for reduction of the $Z_{1/2}$ and $EH_{6/7}$ centers during oxidation. Interstitials generated at the SiO_2/SiC interface diffuse into SiC bulk, and occupy carbon vacancies related to the $Z_{1/2}$ and $EH_{6/7}$ centers.

oxidation-time dependence, and initial-$Z_{1/2}$-concentration dependence of the defect reduction in both n-type and p-type 4H-SiC epilayers. Based on these data, an analytical model of defect reduction as well as the most effective way to reduce the $Z_{1/2}$ center are proposed. In addition, the effect of the $Z_{1/2}$ reduction on the carrier lifetime is investigated through the relation between the carrier lifetime and the $Z_{1/2}$ depth-profile after the oxidation process under various conditions.

II. EXPERIMENTS

The starting materials were n-type (N_d: 10^{14}–10^{15} cm^{-3}) and p-type (N_a: 10^{15}–10^{16} cm^{-3}) 4H-SiC (0001) epilayers. A series of samples was oxidized at different temperatures (1150–1400 °C) for various times (1.3–16.5 h) in 100% oxygen ambient, while the other set of samples was implanted with 10–50 keV carbon ions with a total dose of 1×10^{13} cm^{-2} or 1×10^{14} cm^{-2} (implanted atom concentration: 1×10^{18} cm^{-3} or 1×10^{19} cm^{-3}), forming a 140-nm-box-profile. The C^+-implanted samples were annealed in Ar ambient at various temperatures (1000–1800 °C) for 20 min. For DLTS measurements, Ni and Ti were employed as Schottky contacts on n-type and p-type samples, respectively. The typical diameter of Schottky contacts was 1 mm. A Ti/Al/Ni (20 nm/100 nm/80 nm) layer annealed at 1000 °C for 2 min was employed as backside ohmic contacts for p-type materials. A period width of 0.205 s was employed for all DLTS measurements performed in this study. The depth profiles of deep-level concentrations until 10-μm depth were measured by changing the reverse bias voltage up to 100 V in DLTS measurements. To monitor deeper regions (over 10 μm), the samples were mechanically polished from the surfaces, and DLTS measurements were repeated. It was confirmed that additional deep levels did not appear after the polishing. The carrier lifetime was measured at room temperature by microwave photoconductance decay (μ-PCD) equipped with an yttrium lithium fluoride-third harmonic generation laser ($\lambda = 349$ nm) as an excitation source.

III. RESULTS AND DISCUSSION

A. Defect distributions after trap reduction processes

At first, deep levels after the two trap-reduction processes are compared. Figure 2 and 3 shows the DLTS spectra of the n-type/p-type samples after dry oxidation at 1300 °C

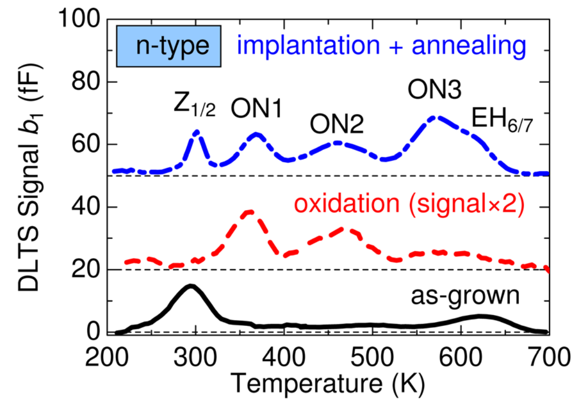

FIG. 2. (Color online) DLTS spectra of the n-type 4H-SiC after thermal oxidation at 1300 °C for 1.3 h (dashed line) and C^+ implantation followed by Ar annealing at 1800 °C for 20 min (dashed-dotted line).

for 1.3 h, as well as the samples after C^+ implantation (dose: 1×10^{14} cm^{-2}) and subsequent Ar-annealing at 1800 °C/1300 °C for 20 min. Here, the signal b_1 is the coefficient of the first sine term in the Fourier series of deep level transient Fourier spectroscopy.[25] After the C^+-implantation process (dashed-dotted lines), the new peaks, ON1 (E_C – 0.84 eV), ON2 (E_C – 1.1 eV), and ON3 (E_C – 1.6 eV) in n-type SiC (Fig. 2), and HK0 (Refs. 4 and 26) (E_V + 0.79 eV) in p-type SiC (Fig. 3), appeared, while the same four peaks are also observed after thermal oxidation (dashed lines). The ON1 and ON2 centers should correspond to the deep levels reported as "new traps" in SiC after C^+-implantation process.[20] On the other hand, two major deep levels, $Z_{1/2}$ (E_C – 0.67 eV) and $EH_{6/7}$ (E_C – 1.6 eV), are reduced in n-type SiC after thermal oxidation as shown by the dashed line in Fig. 2. The $Z_{1/2}$ and $EH_{6/7}$ centers are also reduced to below the detection limit by C^+ implantation followed by Ar annealing at 1500 °C (not shown), while they are regenerated by high-temperature (over 1700 °C) annealing as shown by the dashed-dotted line in Fig. 2. The reduced deep levels as well as generated levels by the trap-reduction processes are summarized in Table I. The defect behaviors (generation and reduction) for thermal oxidation clearly agree with those for the C^+-implantation process, which indicates that similar phenomena (such as interstitial diffusion) may occur in the two processes.

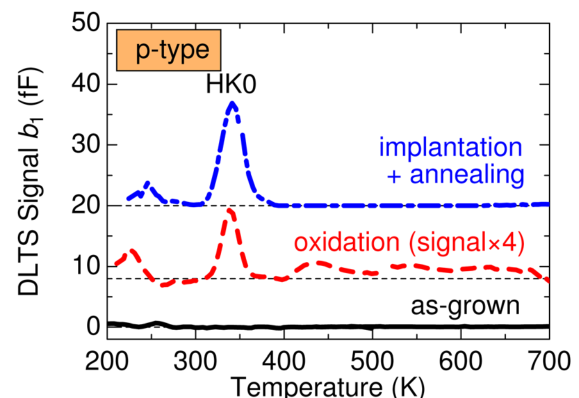

FIG. 3. (Color online) DLTS spectra of the p-type 4H-SiC after thermal oxidation at 1300 °C for 1.3 h (dashed line) and C^+ implantation followed by Ar annealing at 1300 °C for 20 min (dashed-dotted line).

Downloaded 07 May 2012 to 130.54.110.71. Redistribution subject to AIP license or copyright; see http://jap.aip.org/about/rights_and_permissions

TABLE I. Reduced and generated defects in SiC by C^+-implantation process and by thermal oxidation. The conduction types of the samples where each defect is observed are shown in parentheses.

C^+ implantation + Ar annealing		Thermal oxidation	
Reduced defects	Generated defects	Reduced defects	Generated defects
$Z_{1/2}$ (n-type) $EH_{6/7}$ (n-type)	ON1 (n-type) ON2 (n-type) ON3 (n-type) HK0 (p-type)	$Z_{1/2}$ (n-type) $EH_{6/7}$ (n-type)	ON1 (n-type) ON2 (n-type) ON3 (n-type) HK0 (p-type)

It is important to investigate the depth profiles of generated and reduced defects in order to understand what phenomena occur during the trap-reduction processes. Figure 4 shows the depth profiles of ON1 center (generated defect) after oxidation at various temperatures for 1.3 h. With increasing oxidation temperature, the ON1 concentration increases and is distributed to a deeper region, suggesting that the ON1 center is related to the atoms, most likely interstitials, diffused from the SiO_2/SiC interface. The ON2 and HK0 centers (generated defects) showed similar behavior (not shown). Figure 5 shows the depth profiles of $Z_{1/2}$ center (reduced defect) after oxidation at various temperatures for 1.3 h. In this particular case, the initial $Z_{1/2}$ concentration was increased to 1.7×10^{14} cm^{-3} by electron irradiation (energy: 150 keV, fluence: 1×10^{17} cm^{-2}) in order to investigate trap reduction in the sample with high initial-$Z_{1/2}$-concentration. With increasing oxidation temperature, the $Z_{1/2}$ concentration decreases and is eliminated to a deeper region, suggesting that the $Z_{1/2}$ center is related to the (carbon) vacancies, which are occupied by diffused interstitials during oxidation. In addition, the depth of the $Z_{1/2}$-elimination region is proportional to the square root of the oxidation time ($t_{ox}^{1/2}$).[21] These results clearly suggest that the diffusion phenomena is taking place in the SiC bulk region during thermal oxidation.

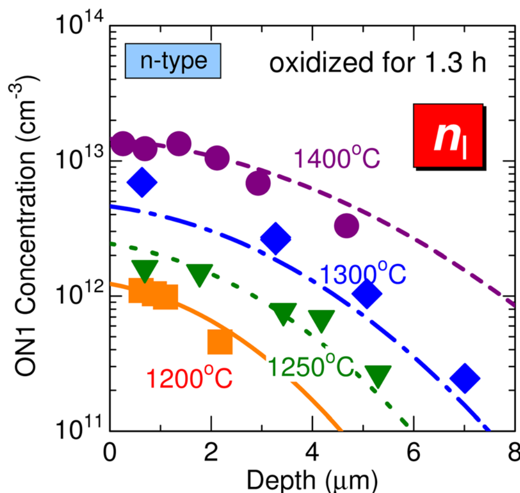

FIG. 4. (Color online) Depth profiles of ON1 center after oxidation at various temperatures for 1.3 h. Each symbol indicates the experimental data and each line indicates the calculated n_I distribution obtained from Eqs. (1)–(8).

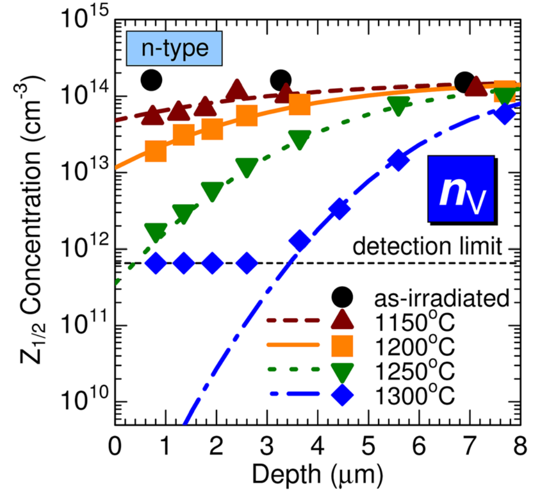

FIG. 5. (Color online) Depth profiles of $Z_{1/2}$ center after oxidation at various temperatures for 1.3 h. The initial $Z_{1/2}$-concentration is 1.7×10^{14} cm^{-3}. Each symbol indicates the experimental data and each line indicates the calculated n_V distribution obtained from Eqs. (1)–(8).

B. Analytical model for defect distributions after thermal oxidation

As discussed above, the reduction of the $Z_{1/2}$ center by oxidation can be explained by diffusion of interstitials and recombination with vacancies as shown in Fig. 1. Therefore, to predict defect distributions after thermal oxidation, the following diffusion equations are solved.

Evolution equations

$$\frac{\partial n_I}{\partial t} = D \cdot \frac{\partial^2 n_I}{\partial x^2} - \gamma \cdot n_I \cdot n_V, \tag{1}$$

$$\frac{\partial n_V}{\partial t} = -\gamma \cdot n_I \cdot n_V. \tag{2}$$

Boundary and initial conditions

$$-D \cdot \frac{\partial n_I}{\partial x}\Big|_{x=0} = F_0 \cdot t^{-\alpha} (t \neq 0), \tag{3}$$

$$n_I|_{t=0} = 0, \tag{4}$$

$$n_V|_{t=0} = n_{V0}. \tag{5}$$

Fitting parameters

$$D = D_\infty \cdot \exp\left(-\frac{E_{aD}}{kT}\right), \tag{6}$$

$$F_0 = F_{0\infty} \cdot \exp\left(-\frac{E_{aF}}{kT}\right), \tag{7}$$

$$\gamma = \gamma_\infty \cdot \exp\left(-\frac{E_{a\gamma}}{kT}\right), \tag{8}$$

where n_I and n_V are the concentrations of interstitials and vacancies, latter of which is related to the origin of $Z_{1/2}$ center. D denotes the diffusion coefficient of the interstitials, and γ is the recombination coefficient between an interstitial and a vacancy. In this model, vacancies are assumed to be

Downloaded 07 May 2012 to 130.54.110.71. Redistribution subject to AIP license or copyright; see http://jap.aip.org/about/rights_and_permissions

immobile and decrease through the recombination with diffused interstitials as described in Eq. (2). Equation (3) indicates the boundary condition of interstitial emission at the oxidation interface, which is described with F_0: flux of interstitials emitted from the SiO_2/SiC interface when $t_{ox} = 1$ s (t_{ox}: oxidation time). Since the oxidation rate becomes slow with the time, the gradual decrease in flux of emitted interstitials as the oxidation (time) proceeds is considered by introducing a slowdown coefficient α. The flux of interstitials should be in proportion to the oxidation rate. The slowdown of the oxidation reaction at the interface can be estimated from Fig. 6, which shows the dependence of the oxide growth rate on oxidation time at different oxidation temperatures. A result on oxidation at 1100 °C reported by Hijikata *et al.* (Ref. 22) is also plotted in the same figure. When the slope of the plot is described as -α, the oxidation rate is proportional to $t_{ox}^{-\alpha}$. Therefore, interstitial emission can be assumed to decrease in proportion to $t_{ox}^{-\alpha}$ as shown in Eq. (3). For simplicity, the time-dependent oxidation-rate is expressed in two stages; high-oxidation-rate stage ($t_{ox} < 0.8$ h), where α is unity for 1150–1300 °C oxidation and 0.48 for 1400 °C oxidation; and low-oxidation-rate stage (0.8 h $< t_{ox}$), where α is 0.23 for 1150–1300 °C oxidation and 0.48 for 1400 °C oxidation. It is assumed that n_I before oxidation is negligible compared with that after oxidation as described in Eq. (4). A parameter n_{V0} in Eq. (5) denotes the initial vacancy distribution before oxidation. As shown in Eqs. (6)–(8), each parameter is described as a function of temperature. The parameters, E_{aD}, E_{aF}, and $E_{a\gamma}$, indicate the activation energy corresponding to the energy barrier for migration of interstitials, that for generation of interstitials, and that for recombination of interstitials with vacancies, respectively.

C. Comparison between experimental $Z_{1/2}$ profile and calculated vacancy profile after thermal oxidation

Based on Eqs. (1)–(8), the depth profiles of n_I and n_V can be calculated, which are dependent on six fitting parameters: E_{aD}, D_∞, E_{aF}, $F_{0\infty}$, $E_{a\gamma}$, and γ_∞. As mentioned, the authors experimentally obtained the depth profiles of $Z_{1/2}$ concentration after oxidation at different temperatures for several samples with different initial $Z_{1/2}$ concentrations. Symbols in Figs. 5 and 7 show the experimental results for the samples with an initial $Z_{1/2}$ concentration of 1.7×10^{14} cm^{-3} and 2.0×10^{13} cm^{-3}. These experimental depth profiles of $Z_{1/2}$ concentration were fitted with the n_V profiles calculated from Eqs. (1)–(8). In the calculation, arbitrary n_V profile can be obtained by changing D, F_0, and γ. Fig. 8 shows the effects of changing these three parameters, D, F_0, and γ, on the calculated n_V profile. When D becomes higher, n_V becomes relatively higher in the shallow region and lower in the deep region as shown by the dashed line, while opposite phenomena occur in the case of higher γ as shown by the dashed-dotted line. Higher F_0 leads lower n_V in the whole depth region as shown by the dotted line. The fitting parameters are uniquely determined through fitting of a series of $Z_{1/2}$ profiles in the samples with different initial-$Z_{1/2}$-

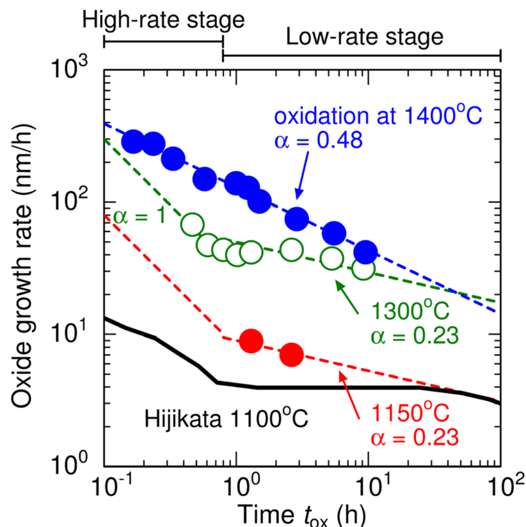

FIG. 6. (Color online) Dependence of the oxide growth rate on oxidation time at different oxidation temperatures. A result (1100 °C) reported by Hijikata *et al.*[22] is also shown as a solid line.

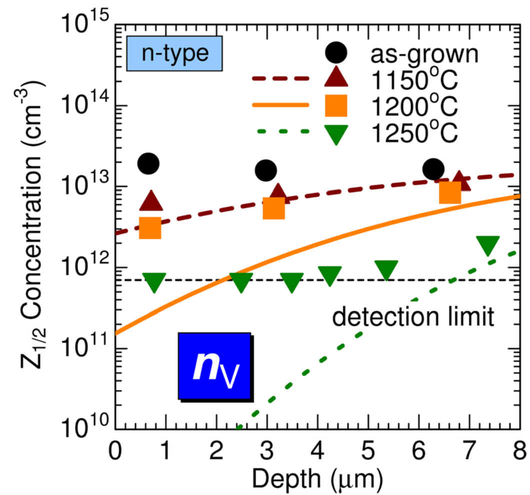

FIG. 7. (Color online) Depth profiles of $Z_{1/2}$ center after oxidation at various temperatures for 1.3 h. The initial $Z_{1/2}$-concentration is 2×10^{13} cm^{-3}. Each symbol indicates the experimental data and each line indicates the calculated n_V distribution obtained from Eqs. (1)–(8).

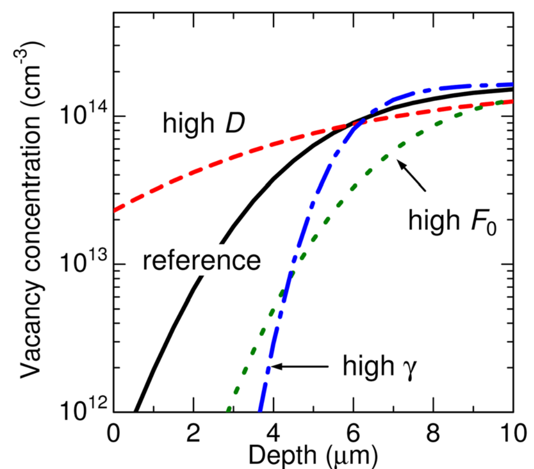

FIG. 8. (Color online) Effects of changing parameters, D, F_0, and γ, on calculated n_V profile. Higher $D/F_0/\gamma$ is used in the calculation for dashed/dotted/dashed-dotted line compared to the calculation for reference (solid line).

Downloaded 07 May 2012 to 130.54.110.71. Redistribution subject to AIP license or copyright; see http://jap.aip.org/about/rights_and_permissions

TABLE II. Parameter values obtained by fitting results of calculated n_V profiles based on Eqs. (1)–(8) and experimental $Z_{1/2}$ profiles shown in Fig. 5. The top row indicates the "X" in the first column.

	D	F_0	γ
Activation energy E_{aX}	0.6 eV	1.4 eV	2.1 eV
Coefficient X_∞	9.7×10^{-9} cm^{2}s^{-1}	4.4×10^{14} cm^{-2}s$^{\alpha-1}$	1.4×10^{-10} cm^{3}s^{-1}

concentration after oxidation at different temperature. The calculated n_V profiles after the fitting are shown as curve lines in Figs. 5 and 7. The obtained values of fitting parameters are summarized in Table II, which are used in all cases in this study. The activation energy for diffusion coefficient (E_{aD}) of interstitials reducing the $Z_{1/2}$ center was determined as 0.6 eV in this study. On the other hand, the migration barrier for carbon/silicon interstitials in n-type SiC has been reported to be (0.5–0.7) eV/(1.4–1.5) eV by Bockstedte *et al*. based on theoretical calculation using density functional theory in the local density approximation,[27] and by Gao *et al*. using molecular dynamics simulations.[28] The activation energy for the diffusion coefficient of interstitials obtained in this study (0.6 eV) agrees with the reported migration energy for carbon interstitials (0.5–0.7 eV), which is consistent with the model that carbon interstitials diffuse from the oxidation interface and fill carbon vacancies.

Using the same parameter values shown in the Table II, the oxidation-time dependence of $Z_{1/2}$ profiles was predicted assuming that the n_V profile corresponds to the $Z_{1/2}$ profile. The results are shown as curved lines in Fig. 9 (initial $Z_{1/2}$ concentration: 1.3×10^{13} cm^{-3}) and Fig. 10 (initial $Z_{1/2}$ concentration: 2×10^{12} cm^{-3}) for 1300 °C oxidation, while corresponding experimental data are shown as symbols in the same figures. The depth profiles of $Z_{1/2}$ concentration after various oxidation conditions show very good agreement with the calculated n_V profiles. (Note that these are not fitted results but the n_V profiles were calculated before experiments.) This agreement indicates the potential to enable prediction of the $Z_{1/2}$ distributions after oxidation at any temperature, for any oxidation time, and any initial $Z_{1/2}$ concentration.

D. Realization of 100-μm $Z_{1/2}$-free region

The authors tried to eliminate the $Z_{1/2}$ center to a 100-μm depth, which is required for 10-kV-class bipolar devices. Figure 11 shows the calculated results of the $Z_{1/2}$ (n_V) profiles for various oxidation times and different initial $Z_{1/2}$ concentrations (2×10^{12} cm^{-3}, 1.3×10^{13} cm^{-3}) using the parameters obtained in this study (Table II). When the initial $Z_{1/2}$ concentration is low, 2×10^{12} cm^{-3}, oxidation at 1300 °C for 30 h is enough for $Z_{1/2}$ elimination in the 100-μm-thick SiC epilayer. However, in the case of high initial $Z_{1/2}$ concentration (>10^{13} cm^{-3}), oxidation over 50 h is required to eliminate the $Z_{1/2}$ center. To minimize the oxidation time, the authors propose three approaches: (i) removing the oxide layer during oxidation, (ii) high-temperature annealing after oxidation, and (iii) higher-temperature oxidation.

(i) Removing the oxide layer during oxidation: In the initial oxidation stage, the interstitial emission rate from the SiO_2/SiC interface is high, as shown in Fig. 6. Therefore, removing the oxide layer during oxidation should promote the interstitial emission and thereby $Z_{1/2}$ reduction. Figure 12 shows the depth profiles of $Z_{1/2}$ center after oxidation at 1300 °C for 15.9 h. Each line indicates an n_V profile calculated with the parameters shown in the Table II, and each symbol indicates experimental data. The rhombuses denote the result for continuous 15.9-h oxidation, and reverse

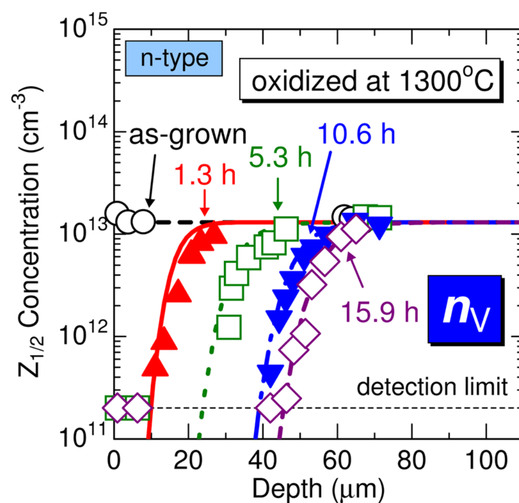

FIG. 9. (Color online) Depth profiles of $Z_{1/2}$ center (initial $Z_{1/2}$-concentration: 1.3×10^{13} cm^{-3}) after oxidation at 1300 °C for 1.3-15.9 h. Each symbol indicates the experimental data and each line indicates the calculated n_V distribution.

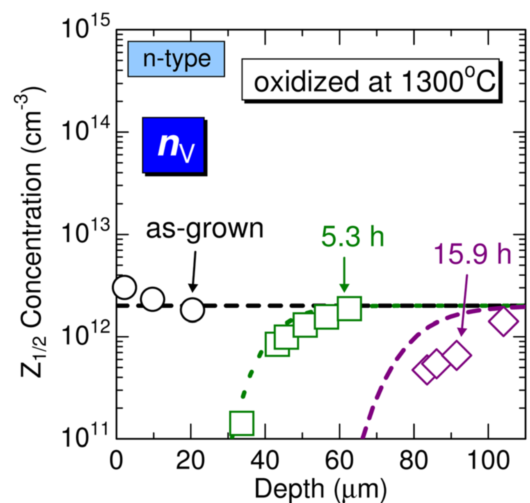

FIG. 10. (Color online) Depth profiles of $Z_{1/2}$ center (initial $Z_{1/2}$-concentration: 2×10^{12} cm^{-3}) after oxidation at 1300 °C for 5.3-15.9 h. Each symbol indicates the experimental data and each line indicates the calculated n_V distribution.

Downloaded 07 May 2012 to 130.54.110.71. Redistribution subject to AIP license or copyright; see http://jap.aip.org/about/rights_and_permissions

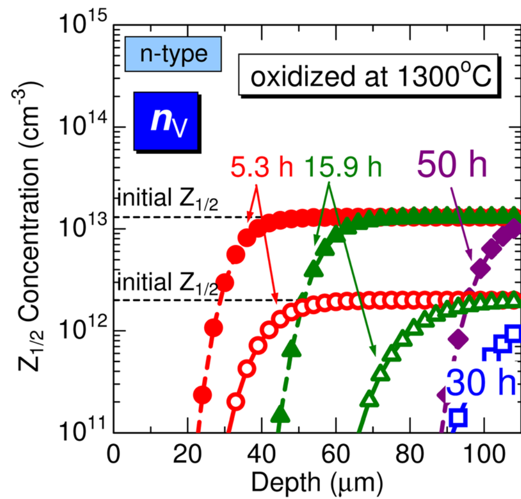

FIG. 11. (Color online) Calculated results of $Z_{1/2}$ profiles for various oxidation times and different initial-$Z_{1/2}$-concentrations (2×10^{12} cm^{-3}, 1.3×10^{13} cm^{-3}) using the parameters obtained in this study. It was assumed that n_V corresponds to the $Z_{1/2}$ concentration.

triangles for 15.9-h oxidation with removing the oxide layer after every 5.3-h oxidation. Removing the oxide layer is clearly effective for enhancing the reduction of the $Z_{1/2}$ center. In the calculation, the effect of removing oxide layer is included by resetting the flux of emitted interstitials, which decreases as the oxidation proceeds, to the initial value after every (in this case 5.3 h) oxidation. The good agreement between experimental data and calculated results again supports the analytical model for trap reduction proposed in this study.

(ii) High-temperature annealing after oxidation: Diffused interstitials should remain in an epilayer after oxidation. Therefore, subsequent high-temperature annealing should enhance diffusion of the residual interstitials to the deeper region and promote $Z_{1/2}$ reduction. Figure 13 shows the $Z_{1/2}$ profiles after oxidation as well as after oxidation

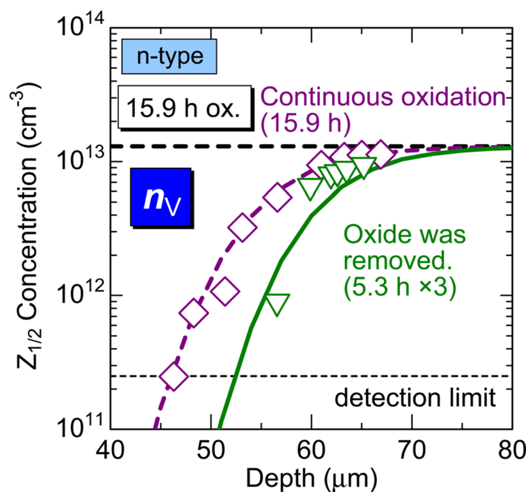

FIG. 12. (Color online) Depth profiles of $Z_{1/2}$ center after oxidation at 1300 °C for 15.9 h. The rhombuses denote the experimental result for continuous 15.9-h oxidation (dashed line: calculated n_V result with the parameters in Table II), and reverse triangles for 15.9-h oxidation with removing the oxide layer after every 5.3-h oxidation (solid line: calculated n_V result with the parameters in Table II).

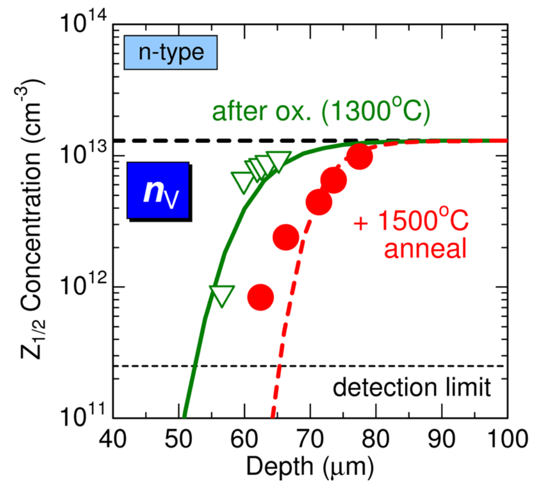

FIG. 13. (Color online) $Z_{1/2}$ profiles after oxidation and after oxidation followed by 1500 °C annealing. The reverse triangles denote the experimental result for after oxidation at 1300 °C for 15.9 h (solid line: calculated n_V result with the parameters in Table II), and the closed circles for the oxidation and subsequent annealing at 1500 °C for 2 h in Ar ambient (dashed line: calculated n_V result with the parameters in Table II).

and subsequent high-temperature (1500 °C) annealing. The solid line indicates the calculated n_V profile just after oxidation at 1300 °C for 15.9 h, and the dashed line denotes that after oxidation and subsequent annealing at 1500 °C for 2 h in Ar ambient. To calculate the effects of Ar annealing at 1500 °C, the same parameters obtained in this study are used except that $F_0 = 0$ (no additional emission of interstitials during the Ar annealing). As shown in Fig. 13, the $Z_{1/2}$ center is eliminated to the deeper region by the subsequent annealing. The experimental data shown as symbols (reverse triangles: after oxidation; closed circles: after oxidation followed by Ar annealing at 1500 °C) clearly agree with the predicted lines, which indicates that the present analytical model is useful for predicting trap distributions not only after oxidation but also after subsequent Ar annealing. In addition, this annealing reduces the HK0 center generated in p-type SiC by thermal oxidation, which also means that residual interstitials further diffuse to the deeper region and promote the $Z_{1/2}$ reduction by the subsequent annealing.

(iii) Higher-temperature oxidation: Because all parameters, D, F_0, and γ, should increase at higher temperature, oxidation at higher temperature must be effective in reduction of the $Z_{1/2}$ centers. Figure 14 shows the depth profiles of $Z_{1/2}$ center after oxidation at 1400 °C for 5.5 h and 16.5 h. Each line indicates the n_V profile calculated with the same parameter values, and each symbol indicates experimental data. The $Z_{1/2}$ centers are eliminated to the depth of about 60 μm after oxidation for 5.5 h, which also agrees with the calculated result. The $Z_{1/2}$ centers could be further reduced but appear to remain at the depth of about 95 μm after oxidation for 16.5 h, while they are completely eliminated in the calculated result. (Calculated n_V distribution after 16.5-h oxidation is not shown because the n_V is lower than 1×10^{10} cm^{-3} in the epilayer.) It should be mentioned that the interface between the epilayer and the substrate is located at the depth of about 96 μm from the surface in this sample. Therefore, the data points near the interface might contain the

Downloaded 07 May 2012 to 130.54.110.71. Redistribution subject to AIP license or copyright; see http://jap.aip.org/about/rights_and_permissions

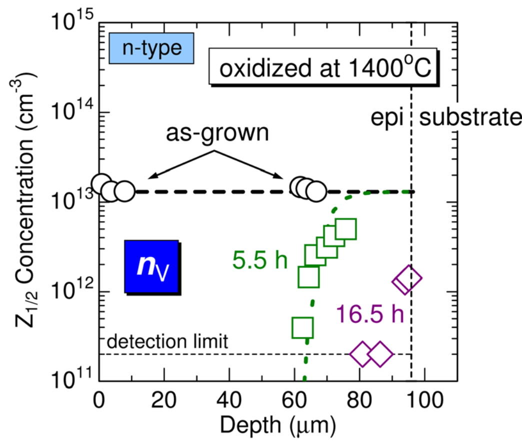

FIG. 14. (Color online) Depth profiles of $Z_{1/2}$ center after oxidation at 1400 °C for 5.5 h and 16.5 h. The dotted line indicates the n_V profile after 5.5-h oxidation calculated with the parameters in Table II and each symbol indicates experimental data. Calculated line for 16.5-h oxidation is not shown because the n_V is lower than 1×10^{10} cm^{-3} in the 96-μm-thick epilayer.

substrate information (high concentration of the $Z_{1/2}$ center must exist in the substrate). Regardless, it was clarified that thermal oxidation at 1400 °C is a very effective way in accelerating $Z_{1/2}$ reduction.

In addition to the above three approaches, higher-rate-oxidation processes such as wet oxidation and plasma oxidation at high temperature may be effective in reducing required oxidation time.

E. Relation between carrier lifetime and $Z_{1/2}$ profile

As mentioned in the introduction, the $Z_{1/2}$ center acts as a lifetime killer in n-type 4H-SiC. Therefore, the deeper region the $Z_{1/2}$ center is eliminated to, the longer carrier lifetime should be. Figure 15 shows μ-PCD decay curves for the 96-μm-thick n-type SiC epilayers (N_d: 2×10^{15} cm^{-3}) on the n-type SiC substrates (thickness: ~350 μm) after different oxidation processes. The oxidation temperature is 1300 °C in Fig. 15 except for the signal labeled "1400 °C." The excitation photon density is 1.1×10^{14} cm^{-2}, which leads to a high

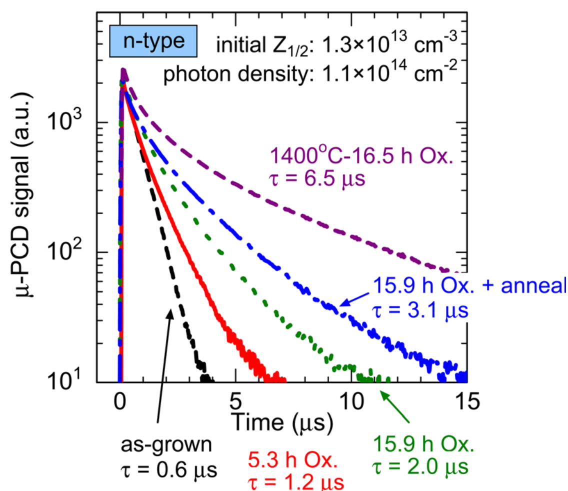

FIG. 15. (Color online) μ-PCD decay curves for the 96-μm-thick n-type 4H-SiC epilayers after different oxidation processes. The oxidation temperature is 1300 °C except for the signal labeled "1400 °C."

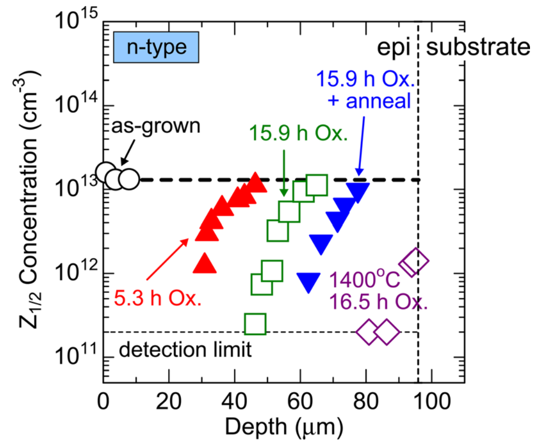

FIG. 16. (Color online) Depth profiles of $Z_{1/2}$ concentration in the same samples as in Fig. 15.

carrier injection level of 10^{16} cm^{-3}. The carrier lifetimes obtained from the decay curves are also described in the figure. The carrier lifetime increased from 0.6 μs (as-grown) to 6.5 μs by oxidation at 1400 °C for 16.5 h. The carrier lifetimes are derived from the slopes of the decay curves at the points where the μ-PCD signals decrease to e^{-3} of the initial intensity because the initial fast decay severely suffers from carrier recombination at the surface and in the substrate.[29–31] Figure 16 indicates the depth profiles of $Z_{1/2}$ concentration in the same samples as in Fig. 15, measured by DLTS. It is obvious that a longer carrier lifetime was obtained in a sample possessing a deeper $Z_{1/2}$-eliminated-region.

Here, the authors tried to quantitatively estimate the relation between the carrier lifetime and the $Z_{1/2}$ profile by a numerical simulation. It has to be noticed that the "measured" carrier lifetime does not represent the true "bulk" carrier lifetime in the epilayer itself because there are other recombination paths of excess carriers. Excess carriers generated by the excitation laser recombine at the surface as well as in the epilayer. The carriers excited in the epilayer also diffuse toward the surface and the substrate due to gradient of the carrier density, which promotes carrier recombination at the surface and in the substrate. Therefore, the measured carrier lifetime contains the effects of carrier diffusion and recombination at the surface, in the epilayer, and in the substrate.[29–31]

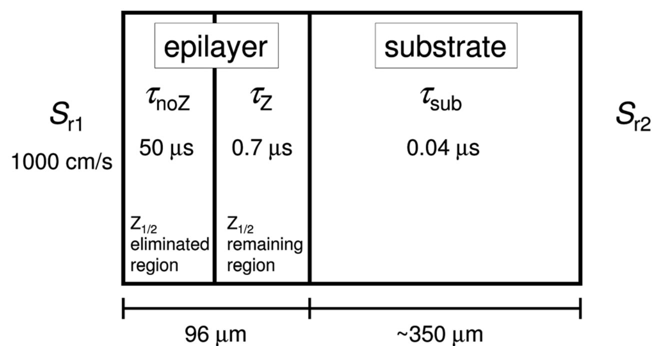

FIG. 17. Schematic illustration of an SiC epilayer grown on an SiC substrate after thermal oxidation. Carrier lifetimes in the $Z_{1/2}$-eliminated region and the $Z_{1/2}$-remaining region are assumed to be 50 μs and 0.7 μs, respectively.

Downloaded 07 May 2012 to 130.54.110.71. Redistribution subject to AIP license or copyright; see http://jap.aip.org/about/rights_and_permissions

TABLE III. Comparison between carrier lifetimes measured by μ-PCD and effective carrier lifetimes predicted by calculation based on a diffusion equation (Ref. 31). Initial $Z_{1/2}$ concentration is 1.3×10^{13} cm^{-3}.

	As-grown	1300 °C-5.3-h Ox.	1300 °C-15.9-h Ox.	1300 °C-15.9-h Ox. + anneal	1400 °C-16.5-h Ox.
Measured by μ-PCD	0.6 μs	1.2 μs	2.0 μs	3.1 μs	6.5 μs
Predicted by calculation	0.6 μs	1.5 μs	2.4 μs	3.2 μs	3.9 μs

In this study, a simulation model,[31] which considers excited-carrier diffusion and recombination in the epilayer, substrate, and at the surface, was employed to estimate the measured carrier lifetimes. An ambipolar diffusion constant of 4.2 cm^2/s (D_{epi})[32] was employed for the epilayer, while a standard hole diffusion constant of 0.3 cm^2/s (D_{sub}) was assumed for the substrate. The optical absorption coefficient at the excitation laser wavelength (349 nm) was obtained as 330 cm^{-1} from the literature.[33] Figure 17 shows a schematic illustration of an SiC epilayer grown on an SiC substrate after thermal oxidation. In this study, the epilayer was divided into two regions, the $Z_{1/2}$-eliminated region ($Z_{1/2}$ concentration $< 2 \times 10^{11}$ cm^{-3}) and the $Z_{1/2}$-remaining region ($Z_{1/2}$ concentration $= 1.3 \times 10^{13}$ cm^{-3} (initial value)). Taking account of results in the literature,[31,34] the bulk carrier lifetime in $Z_{1/2}$-eliminated region (τ_{noZ}) and surface recombination velocity (S_{r1}) were assumed to be 50 μs (Ref. 31) and 1000 cm/s (smooth surfaces were assumed),[34] respectively. Because the backside recombination velocity (S_{r2}) has very little effect on the effective lifetime due to the thick substrate (over 300 μm) and low carrier lifetime in the substrate (0.04 μs), it was assumed as infinity. From the carrier lifetime measured in the as-grown sample, 0.6 μs, the bulk carrier lifetime in the $Z_{1/2}$-remaining region (τ_Z) can be estimated as 0.7 μs. It is mentioned again that the "measured" carrier lifetime, 0.6 μs, is shorter than the "bulk" carrier lifetime, 0.7 μs, due to the recombination at the surface and in the substrate.[35] The boundaries between the $Z_{1/2}$-eliminated region and the $Z_{1/2}$-remaining region were defined to be 35 μm for a sample oxidized at 1300 °C for 5.3 h, 55 μm for oxidized at 1300 °C for 15.9 h, 70 μm for oxidized at 1300 °C for 15.9 h followed by Ar annealing, and 96 μm for oxidized at 1400 °C for 16.5 h from the surface as shown in Fig. 16. By using the simulation model and parameters, "effective" carrier lifetimes (lifetime obtained from a decay curve) were calculated. Table III shows the comparison between the carrier lifetimes measured by μ-PCD and the effective lifetime predicted by the simulation. The predicted effective lifetimes agree well with the measured carrier lifetimes. In the case of 1400 °C oxidation, however, the measured carrier lifetime (6.5 μs) is longer than the predicted carrier lifetime (3.9 μs). The $Z_{1/2}$ center in the substrate near the epilayer/substrate interface might be also reduced by the intensive oxidation, which resulted in longer carrier lifetime.

IV. CONCLUSION

To clarify the mechanism of trap reduction by thermal oxidation, the authors investigated deep levels after two trap-reduction processes, thermal oxidation and C^+ implantation followed by Ar annealing. It was revealed that deep levels generated by thermal oxidation are the same as those generated by C^+ implantation and subsequent Ar-annealing. In addition, the depth profiles of generated/reduced defects represent the distribution of interstitials/vacancies after diffusion phenomena of interstitials from the surface to the SiC bulk region. These results indicate that the same phenomena, diffusion of interstitials, occur during these processes. Furthermore, the authors proposed an analytical model enabling prediction of $Z_{1/2}$ distribution after thermal oxidation using a diffusion equation. This model could reproduce the depth profiles of the $Z_{1/2}$ center in the SiC with different initial-$Z_{1/2}$-concentration after oxidation at any temperature and for any oxidation time. The results suggested that long-time oxidation is required for the elimination of the $Z_{1/2}$ center in the SiC when the initial $Z_{1/2}$-concentration is high. Thus, it is important to keep the initial $Z_{1/2}$-concentration, which depends on the conditions of epitaxial growth and performed device processes, low ($<10^{13}$ cm^{-3}) for achieving long carrier lifetimes. To enhance the $Z_{1/2}$ reduction and reduce process time, three methods, removing the oxide layer during oxidation, 1500 °C annealing after oxidation, and higher-temperature oxidation, were proposed and experimentally proved to be effective. Especially, increasing oxidation temperature was the most effective for enhancement of the $Z_{1/2}$ reduction. Post-oxidation annealing at 1500 °C could reduce the HK0 center, which was generated in SiC epilayers by oxidation. Therefore, to achieve a thick $Z_{1/2}$-free-region for the SiC epilayer with high initial-$Z_{1/2}$-concentration ($>10^{13}$ cm^{-3}), 1400 °C oxidation followed by Ar annealing at 1500 °C is recommended. Creating thick $Z_{1/2}$-free-region clearly improved the carrier lifetime, which agrees well with the values obtained by calculation based on a diffusion equation, which considers excited-carrier diffusion and recombination in the epilayer, in the substrate, and at the surface. By using the analytical models for predictions of $Z_{1/2}$ profile and carrier lifetime, effective carrier lifetimes can be derived from only the depth profile of initial $Z_{1/2}$-concentration and oxidation conditions.

ACKNOWLEDGMENTS

This work was supported by the Funding Program for World-Leading Innovative R&D on Science and Technology (FIRST Program) and a Grant-in-Aid for Scientific Research (21226008) from the Japan Society for the Promotion of Science, and the Global COE Program (C09) from the Ministry of Education, Culture, Sports and Technology, Japan.

[1]T. Dalibor, G. Pensl, H. Matsunami, T. Kimoto, W. J. Choyke, A. Schöner, and N. Nordell, Physica Status Solidi (A) **162**, 199 (1997).

Downloaded 07 May 2012 to 130.54.110.71. Redistribution subject to AIP license or copyright; see http://jap.aip.org/about/rights_and_permissions

[2]C. Hemmingsson, N. T. Son, O. Kordina, J. P. Bergman, E. Janzén, J. L. Lindström, S. Savage, and N. Nordell, J. Appl. Phys. **81**, 6155 (1997).
[3]K. Danno and T. Kimoto, J. Appl. Phys. **100**, 113728 (2006).
[4]K. Danno and T. Kimoto, J. Appl. Phys. **101**, 103704 (2007).
[5]T. Dalibor, H. Trageser, G. Pensl, T. Kimoto, H. Matsunami, D. Nizhner, O. Shigiltchoff, and W. J. Choyke, Mat. Sci. Eng. B **61–62**, 454 (1999).
[6]S. Mitra, M. V. Rao, N. Papanicolaou, K. A. Jones, M. Derenge, O. W. Holland, R. D. Vispute, and S. R. Wilson, J. Appl. Phys. **95**, 69 (2004).
[7]T. Troffer, M. Schadt, T. Frank, H. Itoh, G. Pensl, J. Heindl, H. P. Strunk, and M. Maier, Physica Status Solidi (A) **162**, 277 (1997).
[8]D. Åberg, A. Hallén, and B. G. Svensson, Physica B: Condensed Matter **273–274**, 672 (1999).
[9]Y. Negoro, T. Kimoto, and H. Matsunami, J. Appl. Phys. **98**, 043709 (2005).
[10]K. Kawahara, G. Alfieri, and T. Kimoto, J. Appl. Phys. **106**, 013719 (2009).
[11]K. Kawahara, M. Krieger, J. Suda, and T. Kimoto, J. Appl. Phys. **108**, 023706 (2010).
[12]D. V. Lang and C. H. Henry, Phys. Rev. Lett. **35**, 1525 (1975).
[13]P. B. Klein, B. V. Shanabrook, S. W. Huh, A. Y. Polyakov, M. Skowronski, J. J. Sumakeris, and M. J. O'Loughlin, Appl. Phys. Lett. **88**, 052110 (2006).
[14]K. Danno, D. Nakamura, and T. Kimoto, Appl. Phys. Lett. **90**, 202109 (2007).
[15]L. Storasta, J. P. Bergman, E. Janzén, A. Henry, and J. Lu, J. Appl. Phys. **96**, 4909 (2004).
[16]L. Storasta, A. Henry, J. Bergman, and E. Janzén, Mater. Sci. Forum **457–460**, 469 (2004).
[17]T. Kimoto, S. Nakazawa, K. Hashimoto, and H. Matsunami, Appl. Phys. Lett. **79**, 2761 (2001).
[18]T. Hornos, A. Gali, and B. G. Svensson, Mater. Sci. Forum **679–680**, 261 (2011).
[19]L. Storasta and H. Tsuchida, Appl. Phys. Lett. **90**, 062116 (2007).
[20]L. Storasta, H. Tsuchida, T. Miyazawa, and T. Ohshima, J. Appl. Phys. **103**, 013705 (2008).
[21]T. Hiyoshi and T. Kimoto, Appl. Phys. Expr. **2**, 041101 (2009).
[22]Y. Hijikata, H. Yaguchi, and S. Yoshida, Appl. Phys. Expr. **2**, 021203 (2009).
[23]K. C. Chang, N. T. Nuhfer, L. M. Porter, and Q. Wahab, Appl. Phys. Lett. **77**, 2186 (2000).
[24]J. M. Knaup, P. Deák, T. Frauenheim, A. Gali, Z. Hajnal, and W. J. Choyke, Phys. Rev. B **71**, 235321 (2005).
[25]S. Weiss and R. Kassing, Solid. State Electron **31**, 1733 (1988).
[26]T. Hiyoshi and T. Kimoto, Appl. Phys. Expr. **2**, 091101 (2009).
[27]M. Bockstedte, A. Mattausch, and O. Pankratov, Phys. Rev. B **69**, 235202 (2004).
[28]F. Gao, W. J. Weber, M. Posselt, and V. Belko, Phys. Rev. B **69**, 245205 (2004).
[29]P. B. Klein, R. Myers-Ward, K. Lew, B. L. VanMil, C. R. Eddy, D. K. Gaskill, A. Shrivastava, and T. S. Sudarshan, J. Appl. Phys. **108**, 033713 (2010).
[30]P. Ščajev, V. Gudelis, K. Jarašiūnas, and P. B. Klein, J. Appl. Phys. **108**, 023705 (2010).
[31]T. Kimoto, T. Hiyoshi, T. Hayashi, and J. Suda, J. Appl. Phys. **108**, 083721 (2010).
[32]P. Grivickas, J. Linnros, and V. Grivickas, J. Mater. Res. **16**, 524 (2001).
[33]S. G. Sridhara, R. P. Devaty, and W. J. Choyke, J. Appl. Phys. **84**, 2963 (1998).
[34]M. Kato, A. Yoshida, and M. Ichimura, Jpn. J. Appl. Phys. **51**, 02BP12 (2012).
[35]How to determine the τ_Z: In the case of as-grown samples, the bulk carrier lifetime in the whole region of the epilayer is τ_Z (there is no $Z_{1/2}$-eliminated region). When the bulk carrier lifetime (τ_Z) is assumed to be 0.7 μs, 0.6 μs is obtained as calculated effective lifetime. Because this 0.6 μs is equal to the measured carrier lifetime in as-grown sample, τ_Z is determined to be 0.7 μs.

Downloaded 07 May 2012 to 130.54.110.71. Redistribution subject to AIP license or copyright; see http://jap.aip.org/about/rights_and_permissions